Chemerin receptor blockade improves vascular function in diabetic obese mice via redox-sensitive- and Akt-dependent pathways

Karla Bianca Neves [1,4]; Aurelie Nguyen Dinh Cat [4]; Rheure Alves-Lopes [2,4]; Katie Yates Harvey [4]; Rafael Menezes da Costa [2]; Nubia Souza Lobato [3]; Augusto Cesar Montezano [4]; Ana Maria de Oliveira [1]; Rhian M. Touyz[4]; Rita C Tostes [2].

[1] Department of Physics and Chemistry, Faculty of Pharmaceutical Sciences of Ribeirao Preto, University of Sao Paulo, Ribeirao Preto, SP, Brazil.

[2] Department of Pharmacology, Ribeirao Preto Medical School, University of Sao Paulo, Ribeirao Preto, SP, Brazil.

[3] Department of Biological Sciences, Federal University of Goias, Jatai, GO, Brazil.

[4] Institute of Cardiovascular and Medical Sciences, University of Glasgow, UK.

Running title: Chemerin decreases vascular insulin signaling

* Corresponding author:

Karla Bianca Neves, PhD

Department of Pharmacology

Ribeirao Preto Medical School

University of Sao Paulo, Ribeirao Preto, SP, Brazil.

Tel/Fax: +55-16-3315-3181 / +55-16-3315-4529

e-mail: Karla.Neves@glasgow.ac.uk

ABSTRACT

Chemerin and its G protein-coupled receptor (ChemR23) have been associated with endothelial dysfunction, inflammation and insulin resistance. However, the role of chemerin on insulin signalling in the vasculature is still unknown. We aimed to determine whether chemerin reduces vascular insulin signalling and whether there is interplay between chemerin/ChemR23, insulin resistance and vascular complications associated with type 2 diabetes (T2D). Molecular and vascular mechanisms were probed in mesenteric arteries and cultured vascular smooth muscle cells (VSMC) from C57BL/6J, non-diabetic lean db/m and diabetic obese db/db mice as well as in human microvascular endothelial cells (HMEC). Chemerin decreased insulin-induced vasodilatation in C57BL/6J mice, an effect prevented by CCX832 (ChemR23 antagonist) treatment. In VSMC, chemerin, via oxidative stress- and ChemR23-dependent mechanisms, decreased insulin-induced Akt phosphorylation, GLUT4 translocation to the membrane and glucose uptake. In HMEC, chemerin decreased insulin-activated nitric oxide signalling. AMPK phosphorylation was reduced by chemerin in both HMEC and VSMC. CCX832 treatment of db/db mice decreased body weight, insulin and glucose levels and vascular oxidative stress. CCX832 also partially restored vascular insulin responses in db/db and high fat diet (HFD)-fed mice. Our novel *in vivo* findings highlight chemerin/ChemR23 as a promising therapeutic target to limit insulin resistance and vascular complications associated with obesity-related diabetes.

New & Noteworthy: Our novel findings show that the chemerin/ChemR23 axis plays a critical role in diabetes-associated vascular oxidative stress and altered insulin signaling. Targeting chemerin/ChemR23 may be an attractive strategy to improve insulin signaling and vascular function in obesity-associated diabetes.

Keywords: Adipokines, insulin, vascular smooth muscle, endothelial cells, type 2 Diabetes.

INTRODUCTION

Obesity, characterized by hypertrophy and hyperplasia of adipose tissue, is a critical risk factor for hypertension, dyslipidaemia, cardiovascular disease, and type 2 diabetes (T2D) (33). Obesity is also linked to decreased sensitivity to the biological actions of insulin, a condition identified as insulin resistance (48). In addition to its central energy storage function, adipose tissue secretes several bioactive hormones and cytokines, called adipokines (51). Adipokines have autocrine/paracrine effects that influence not only adipose tissue development and function (21), but also energy homeostasis, glucose and lipid metabolism, food intake, inflammation, and vascular function (26, 51). Dysregulation of adipokine production and secretion contribute to the pathogenesis of obesity and its associated vascular complications (51).

Chemerin, also known as retinoic acid receptor responder protein 2 (RARRES2) or tazarotene-induced gene 2 protein (TIG2), is highly expressed in the placenta, liver, and white adipose tissue (WAT), with a lower expression in tissues such as lung, brown adipose tissue, heart, ovary, kidney, skeletal muscle and pancreas (4, 14). It is secreted as an 18-kDa inactive pro-protein and undergoes extracellular serine protease cleavage to generate the 16-kDa active chemerin (50). Chemerin is a chemoattractant protein that binds to the G protein-coupled receptor CMKLR1 (chemokine-like receptor 1), also known as ChemR23, which is expressed in macrophages, dendritic cells, adipocytes (50) as well as in endothelial and vascular smooth muscle cells (VSMC), as recently reported (46). Although chemerin also activates the G protein-coupled receptor 1 (GPR1) with similar affinity to CMKLR1 and is a ligand for a third receptor, chemokine receptor-like 2 (CCRL2), which does not seem to activate intracellular responses,

essentially all known responses to chemerin have been attributed to the activation of ChemR23 (1).

Chemerin is currently described as a biomarker for adiposity in humans. Circulating chemerin levels were shown to be strongly associated with multiple components of metabolic syndrome, including body mass index (BMI), triglycerides, high-density lipoprotein cholesterol (HDL-C) and hypertension (4), and are also linked to adipogenesis (15, 35). Circulating chemerin levels are increased in numerous diseases associated with chronic inflammation (47). Serum levels of chemerin correlate with levels of proinflammatory cytokines, such as tumor necrosis factor-α (TNF-α), interleukin 6 (IL-6) and C reactive protein (CRP) (24, 47). Importantly, ChemR23 knockout mice present reduced adiposity and body mass (9) and chemerin levels are reduced by weight loss and fat reduction (9). Chemerin expression is upregulated in adipocytes of diet-induced obese mice (10, 34). Increased chemerin expression in WAT, skeletal muscle, and liver has been reported in mouse models of obesity/diabetes and chemerin exacerbates glucose intolerance, lowers serum insulin levels, and decreases tissue glucose uptake in obese diabetic db/db mice (10, 35). More recently, it has also been demonstrated an important role for reactive oxygen species (ROS) in chemerin signalling in vascular cells. Particularly chemerin, through ROS, stimulates mitogenic and pro-inflammatory signalling pathways promoting vascular damage and remodelling (45).

Although chemerin has been shown to impair insulin signalling and to induce insulin resistance in skeletal muscle cells (41) and cardiomyocytes (52), the role of chemerin in vascular insulin resistance particularly in the context of diabetes, has not been fully elucidated. Therefore, the present study aimed to determine whether chemerin influences vascular insulin signalling and whether there is interplay between chemerin/ChemR23, insulin resistance and vascular

complications associated with T2D. We hypothesized that chemerin, through ChemR23, decreases vascular insulin signalling and that ChemR23 antagonism attenuates abnormal vascular responses to insulin in obese diabetic db/db mice.

MATERIALS AND METHODS

All experimental protocols on mice were performed in accordance with the Ethical Principles in Animal Experimentation adopted by the West of Scotland Research Ethics Service and in accordance with the National Institutes of Health Guide for the Care and Use of Laboratory Animals and the National Council for Animal Experimentation Control (CONCEA) and were approved by the Ethics Committee on Animal Use (CEUA) from the University of Sao Paulo (USP) (protocol nº 12.1.1593.53.0).

Animals

Ten to twelve weeks-old male C57BL/6J, lean non-diabetic db/m and obese diabetic db/db mice were housed in individual cages in a room with controlled humidity and temperature (22°C - 24°C), and light/dark cycles of 12 hours (h). Animals had free access to food and tap water. Animals were treated with vehicle (PEG400/cremophor) or CCX832, a ChemR23 antagonist, (a gift from ChemoCentryx, Inc., Mountain View, CA, USA) (75 mg/kg/day, for 3 weeks, by oral gavage). Animals were separated into 4 groups: db/m + vehicle, db/m + CCX832, db/db + vehicle and db/db + CCX832. In initial experiments, in order to confirm that the vehicle had no effects itself, two additional groups were included and maintained for the same three week-period: db/m and db/db mice without any treatment (i.e. untreated db/m and db/db mice).

Since no differences were observed between the untreated and vehicle groups, the remaining protocols were performed in animals treated with vehicle or CCX832. In another set of experiments, six week-old male C57BL/6J mice were maintained either on a control diet (protein 22%, carbohydrate 70% and fat 8% of energy, PragSolucoes, Jau, Brazil) or on a high-fat diet [(HFD), protein 10%, carbohydrate 25% and fat 65% of energy, PragSolucoes] for 18 weeks.

Insulin sensitivity was calculated using the HOMA-IR index (Homeostasis Model Assessment), which takes into account insulin and fasting blood glucose levels, using the following mathematical formula: HOMA-IR = fasting insulin × fasting glucose/22.5. Additional nutritional and metabolic information from the mouse models can be found in previous studies (6, 7, 42). At the end of treatment animals were maintained under anaesthesia with 2.5% isoflurane for blood collection and then culled by carbon oxide (CO_2) inhalation.

Cultured Vascular Cells

Vascular smooth muscle cells (VSMC) from mesenteric arteries of C57BL/6J mice were isolated and characterized as previously described (45). Sub confluent cell cultures were rendered quiescent by serum deprivation for 24 h before experimentation. Low-passage cells (passages 4–6) from different primary cultures were used in our experiments.

Human microvascular endothelial cells (HMEC) (Life Technologies, Carlsbad, CA, USA) were also studied. Endothelial cells were cultured in Medium 131 supplemented with Microvascular Growth Supplement (MVGS; 25 ml), Gentamicin (50 µg⁄ml) and Amphotericin B (0.25 µg⁄ml). For functional studies, confluent cells were quiescent for 4 hours in low-serum medium containing 0.5% FBS and subsequently stimulated according to the experimental protocol. Four to six different batches of endothelial cells were studied for each experiment.

Cells were stimulated with recombinant chemerin (R&D Systems - 0.5 ng/mL). When inhibitors were used in any protocol, parallel experiments were performed to determine the effects of the inhibitor itself. Data were included in the graphics only if the inhibitor by itself produced a significant effect.

Plasma Biochemistry

Mice were fasted for 12 h and blood was collected immediately prior to sacrifice in tubes containing heparin. After collection, plasma was separated by centrifugation (2,000 rpm, 10 min). Plasma was aliquoted, snap frozen and storage at -80 ^{o}C. Glucose, cholesterol and triglycerides were determined by an automated analyser (Roche/Hitachi cobas c systems - cobas c 311 Autoanalyser).

Chemerin and insulin levels

Chemerin and insulin plasma levels were determined by ELISA, according to instructions from the manufactures (Cat. No. MCHM00 - R&D Systems and 10-1247-01 – Mercodia, respectively).

Functional studies in mesenteric arteries

First- and second-order mesenteric resistance arteries from C57BL/6J, db/m and db/db mice, as well as from mice treated with a control or a HFD for 18 weeks, were cut into 2 mm ring segments and mounted in a wire myograph, as previously described (16). Myograph chambers were filled with 5 mL of physiological solution [(in mmol/L): 130 NaCl, 14.9 $NaHCO_3$, 4.7 KCl, 1.18 KH_2PO_4, 1.17 $MgSO_4 \cdot 7H_2O$, 5.5 glucose, 1.56 $CaCl_2 \cdot 2H_2O$, and 0.026

EDTA] and continuously gassed with a mixture of 95% O_2 and 5% CO_2 at a temperature of 37º C. After 30 min of stabilization, the contractile ability of the preparations was assessed by adding KCl (120 mmol/L) to the organ baths. Endothelial integrity was verified by relaxation induced by acetylcholine (1 µmol/L; ACh) in vessels pre-contracted with phenylephrine (2 µmol/L; PhE). Concentration-effect curves to human regular insulin (Eli Lilly®, Sao Paulo, Brazil) were performed in arteries from all animal groups. In some experiments, the vascular preparations were incubated with Tiron (ROS scavenger, 100 µmol/L), CCX832 (ChemR23 antagonist, 10 nmol/L) or YS-49 (PI3K activator, 1 µmol/L). For the HFD mice, CCX832 was added to the chamber 30 minutes prior the curves.

Immunoblotting

Western blotting was developed in cultured VSMC from C57BL/6J and aorta from db/m and db/db mice treated with vehicle or CCX832 as previously described (45). The mesenteric arteries were not further explored for other experiments due to the limitation of the amount of tissue. Briefly, tissues were homogenized in lysis buffer [(in mmol/L) sodium pyrophosphate 50, NaF 50, NaCl 5, EDTA 5, EGTA 5, HEPES 10, Na_3VO_4 2, PMSF 50, Triton 100 0.5%, and leupeptin/aprotinin/pepstatin 1 mg/mL) and then sonicated for 5 sec. Proteins (50 – 60 µg) extracted from each lysate were separated by electrophoresis on SDS polyacrylamide gel and transferred to a nitrocellulose membrane. Nonspecific binding sites were blocked with 5% milk in Tris-buffered saline solution with Tween (TBS-T) for one hour at room temperature. Primary antibodies were diluted in TBS-T containing 3% of BSA and incubated overnight at 4ºC. After incubation for one hour with secondary antibodies in room temperature, signals were revealed with chemiluminescence, visualized by autoradiography and quantified densitometrically with

open-source software ImageJ (http://imagej.nih.gov/ij/). Results were normalized by β-actin, α-tubulin or respective total proteins. Antibodies were used as follow: anti-eNOS [9572], anti-phospho eNOS [9571], anti-phospho Akt [9271], anti-Akt [9272], anti-phospho PI3K [4228], anti-phospho AMPK [2531], anti-AMPK [2532]; anti-GLUT4 [07-1404] (Millipore; 1:1000); anti Na^+/K^+ ATPase (3010 Cell Signaling; 1:10000); anti-α-tubulin [T6074] and anti-β-actin [A2228] (Sigma; 1:10000).

Isolation of membrane and cytosolic fractions

After stimulation, VSMC were treated with ice-cold hypotonic lysis buffer (10 mmol/l Tris, pH 7.4, 1.5 mmol/l $MgCl_2$, 5 mmol/l KCl, 1 mmol/l DTT, 0.2 mmol/l sodium vanadate, 1 mmol/l PMSF, 1 g/ml aprotinin, 1 g/ml leupeptin). After passing the lysate through a 25-gauge syringe needle with several rapid strokes, the samples were centrifuged at 2,000 *g* at 4ºC for 5 min. The supernatant was recentrifuged at 100,000 *g* at 4°C for 60 min. The pellet was resuspended in lysis buffer containing 0.1% Triton X-100 and served as the membrane fraction. Proteins were measured by the Bradford method using BSA as the standard. Membrane fraction was used to perform western blot analysis for glucose transporter-4 (GLUT4) translocation.

Immunofluorescence

Paraffin sections of aorta (4 µm) were deparaffinised in xylene, rehydrated through graded ethanol, and washed in water. All sections were incubated in EDTA (pH 8) and boiled for 15 min at 95°C for antigen unmasking. Slides were cooled to room temperature, permeabilized in 0.5% Triton X-100 in PBS for 5 min, and blocked with 10% donkey serum, 1% BSA in 1xTBS-T for one h at room temperature in a humidified chamber. For 8-hydroxyguanosine (8-

OHG) immunostaining, slides were incubated overnight with anti- 8-OHG goat polyclonal antibody (Abcam ab10802, 1:200) in a humidified chamber. Alexa-fluor-488-conjugated donkey anti-goat secondary antibody (Molecular probes, A-11055, 1:300) was used after primary antibody incubation for 1 h at room temperature in the dark. The slides were treated with 0.1% Sudan Black B (Sigma Aldrich, 199664) in methanol for 10 min in order to remove lipofuscin-mediated autofluorescence. Nuclei were counterstained with 4-6-diamidino-2-phenylindole (DAPI at 100 µg/ml) for 10 min. Sections were mounted with a coverslip using ProLong Gold anti-fade mounting media containing DAPI (Molecular probes, P-36931) in the dark. Fluorescence images were captured using Axiovert 200M microscope with a laser-scanning module LSM 510 (Carl Zeiss AG, Heidelberg, Germany). Fluorescence quantification was performed using the open-source software ImageJ (http://imagej.nih.gov/ij/) and determined by the average of five different fields captured from each vessel. For negative controls, goat IgG-matched isotype controls were used (Santa Cruz, sc-2028).

Nitric oxide production

Production of nitric oxide (NO) was determined with the NO fluorescent probe diacetate 4-amino-5-methylamino-2',7'-difluorofluorescein diacetate (DAF-2AM - Life Technologies, Carlsbad, CA, USA) as previously described (45). Endothelial cells were incubated with DAF-FM diacetate (5 µmol/L, 30 min) in serum free media, kept in the dark, and maintained at 37ºC. Cells were washed to remove excess probe and an additional incubation for 10 min was performed to allow complete de-esterification of the intracellular diacetates. Cells were stimulated with chemerin (R&D Systems - 0.5 ng/mL) for one hour and insulin (100 nmol/L), CCX832 (10 nmol/L), N-acetyl-cysteine (NAC; 10 µmol/L) and 740Y-P (PI3K/Akt signalling

activator; 1 μmol/L) for 30 min. After stimulation, cells were washed with PBS and harvested by mild trypsinization (trypsin - 0.025%). Trypsin was inactivated with soybean trypsin inhibitor (0.025%) in PBS (1:1). Additional PBS (37ºC) was added to final volume of 10 mL. Cells were centrifuged for 3 min at 3,000 g. Following centrifugation, the supernatant was discarded, and the cell pellet reconstituted in PBS (250 μl). 200 μl of the cell suspension was transferred to black 96 well microplates (Nunc® 436034). The DAF-FM nitrosylation was assessed by a fluorimeter at excitation/emission wavelengths of 495/515 nm. Fluorescence intensity was adjusted to protein concentration.

Glucose uptake measurement

VSMC were exposed to chemerin or vehicle, CCX832, Tiron, AICAR (AMPK signalling activator; 1 mmol/L) or 740Y-P in the presence of insulin stimulation and then incubated with buffer Krebs-Ringer-Hepes (15 mmol/L Hepes [pH 7.4], 105 mmol/L NaCl, 5 mmol/L KCl, 1.4 mmol/L $CaCl_2$, 1 mmol/L KH_2PO_4, 1.4 mmol/L $MgSO_4$ and 10 mmol/L $NaHCO_3$) for 2 hours. The cells were incubated with insulin (100 nmol/L) for 30 min and 0.2 mmol/L glucose 2-deoxy-D-glucose containing 1 μCi/ml of 2-deoxy-D- [3^H] -glucose was added over 30 min. The buffer was rapidly removed, followed by three washes with ice-cold PBS. Cells were lysed with 500 μL of 0.4 mol/L NaOH for 5 min and neutralized with 500 μL of HCl. The amount of radiolabeled glucose associated with the lysed cells was determined by liquid scintillation counting. To control for changes in osmotic pressure, the effect of insulin on 14^C-mannitol uptake was also determined.

Data and statistical analysis

All data are expressed as mean±SEM. Relaxation responses are expressed as a percentage of contraction in response to PhE. The individual concentration–response curves were fitted into a curve by non-linear regression analysis. *p*D2 (defined as the negative logarithm of the EC_{50} values) and maximal response (Emax) values were compared by one-way analysis of variance (ANOVA) followed by the Tukey post hoc test. The Prism software, version 5.0 (GraphPad Software Inc., San. Diego, CA, USA) was used to analyze these parameters as well as to fit the sigmoidal curves. To analyze the difference between the two groups an unpaired *t*-test was used. N represents the number of animals or experiments used and *p* values less than 0.05 were considered significant.

RESULTS

Chemerin decreases insulin-induced dilatation of mesenteric resistance arteries

As shown in Figure 1A, chemerin decreased insulin-induced relaxation of mesenteric arteries from C57BL/6 mice, an effect blocked by the ChemR23 antagonist CCX832 (Figure 1B). An activator of PI3K signalling (YS-49) and a ROS scavenger (Tiron) reversed chemerin effects on insulin-induced vasodilatation (Figures 1C and 1D).

Chemerin decreases insulin-induced NO signalling activation in endothelial cells

To verify whether chemerin affects NO signalling, HMEC were exposed to chemerin (0.5 mg/ml) and probed for eNOS phosphorylation. Chemerin decreased basal and insulin-induced eNOS phosphorylation of the active site (Ser^{1177}) (Figure 1E). These effects were attenuated both

by a ROS scavenger (N-acetyl-l-cysteine – NAC) and a PI3K activator (740Y-P) (Figure 1E), indicating that oxidative stress mechanisms and insulin-downstream signalling are involved in chemerin-induced decreased NO bioavailability, leading to endothelial dysfunction.

To determine whether reduced eNOS phosphorylation was associated with decreased NO production, levels of NO were estimated in insulin and chemerin-stimulated HMEC. Chemerin decreased NO levels in HMEC. Insulin increased NO levels in these cells and, in the presence of chemerin, insulin-induced NO production was significantly reduced. This effect involves ChemR23-, PI3K signalling- and ROS-dependent mechanisms since CCX832, 740Y-P and NAC partially inhibited chemerin effects (Figure 1F).

Chemerin decreases insulin signalling in VSMC

In addition to its effects on endothelial cells, chemerin decreased insulin signalling in VSMC. Insulin increased Akt phosphorylation in VSMC and chemerin decreased insulin-induced Akt phosphorylation via ChemR23 and ROS-dependent mechanisms (Figure 2A).

To further investigate chemerin effects on insulin signalling, GLUT4 translocation from the intracellular membrane compartments to the membrane was determined. In VSMC, chemerin decreased insulin-induced GLUT4 translocation to the membrane (Figure 2B), which was blocked by CCX832 and 740Y-P (Figure 2B). This suggests that ChemR23 and PI3K activation is contributing to the chemerin effects on GLUT4 translocation in VSMC.

Chemerin reduces insulin-stimulated glucose uptake by VSMC

We evaluated the effects of chemerin on AMPK phosphorylation, another mechanism for glucose uptake. Chemerin decreased AMPK phosphorylation (Thr^{172}) both in VSMC and HMEC

(Figures 2C and 2D). To evaluate whether chemerin also affects insulin-induced glucose uptake, 2-deoxyglucose uptake was measured in VSMC exposed to 2 μCi/ml 2-[^{3}H]DG in the presence of unlabelled 2-DG. In VSMC, chemerin decreased insulin-induced glucose uptake (Figure 3) through ROS generation, AMPK and PI3K/Akt signalling since Tiron, AICAR, CCX832 and 740Y-P reversed the effects of chemerin on glucose transport (Figure 3).

ChemR23 antagonism decreases body weight and insulin and glucose levels in db/db mice

Since chemerin influences vascular insulin signalling, we investigated whether ChemR23 antagonism attenuates diabetes-related vascular dysfunction and insulin resistance. Plasma chemerin levels were significantly increased in diabetic obese db/db mice (Figure 4A). CCX832 treatment slightly reduced body weight of db/db mice when compared to vehicle-treated db/db mice (Figure 4B). In addition, CCX-treated db/db mice exhibited decreased plasma levels of glucose and insulin *vs*. vehicle-treated db/db mice (Figures 4C and 4D). The HOMA index indicated that CCX832 improves insulin sensitivity in db/db mice (Figure 4E). Increased cholesterol and triglyceride levels in db/db mice were reduced by CCX832. No differences in the lipid profile were observed in db/m mice treated with vehicle or CCX832 (Figures 4F and 4G).

CCX832 partially reverses dysfunctional insulin responses in vessels from db/db mice

As shown in Figure 5A, insulin-induced dilation was decreased in mesenteric arteries from vehicle-treated db/db mice *vs*. vehicle-treated db/m mice. CCX832 treatment partially improved insulin-induced vasodilation in db/db mice (Figure 5A). Moreover, Akt (Ser^{473}) phosphorylation was reduced in aorta from vehicle-treated db/db mice *vs*. vehicle-treated db/m

mice and CCX832-treated db/db mice (Figure 5B), indicating beneficial effects of *in vivo* treatment with CCX832 on insulin signalling.

Additionally, as observed in Figure 5C, increased levels of chemerin were also observed in HFD-fed mice. The ChemR23 antagonist CCX832 attenuated impaired insulin-induced dilatation in mesenteric arteries from HFD-fed mice (Figure 5D).

CCX832 reduces vascular oxidative stress in db/db mice

Considering that chemerin increases ROS generation (45) and that oxidative stress accounted for most of the effects of chemerin upon vascular insulin signalling, we investigated whether ChemR23 antagonism attenuates ROS generation in db/db mice. Diabetic mice presented increased vascular levels of DNA oxidation products in comparison to vehicle- and CCX832-treated db/m mice (Figures 6A and 6B). This was reduced by treatment of db/db mice with CCX832 (Figures 6A and 6B).

DISCUSSION

Our results demonstrated that (1) chemerin decreases insulin-induced vasodilation by mechanisms involving ChemR23 activation, disruption of PI3K/Akt signalling and oxidative stress; (2) chemerin decreases insulin-induced eNOS phosphorylation and NO production in endothelial cells through mechanisms that affect ROS generation and PI3K/Akt signalling; (3) chemerin decreases activation of insulin signalling pathways via ChemR23 and oxidative stress in VSMC; (4) ChemR23 antagonism with CCX832 decreases glucose and insulin levels in db/db mice; (5) CCX832 partially restores insulin-induced vasodilatation and improves insulin

signalling in diabetic obese mice; (6) CCX832 decreases vascular oxidative stress in db/db mice. These novel findings show that the chemerin/ChemR23 axis plays a critical role in diabetes-associated vascular oxidative stress and altered insulin signalling.

Chemerin was first described as a chemoattractant agent, promoting chemotaxis of leukocyte populations that express ChemR23. Later on, chemerin was associated with regulation of key effectors of the glucose and lipid metabolism in mature adipocytes (11) as well as a regulator of adipogenesis in 3T3-L1 cells (14). Regarding vascular homeostasis, chemerin has been shown to promote proliferation of endothelial cells and release of MMP-2 and MMP-9, suggesting a contribution of the chemerin/ChemR23 system in angiogenesis. In co-cultures of fibroblast and endothelial cells, chemerin promotes the formation of endothelial tubules in a MAPK-dependent manner (8). On the other hand, in obesity, production of adipokines triggers chronic inflammation and leads to increased levels of proinflammatory cytokines (20), which can modify insulin signalling. TNF-α and IL-6, for example, are good predictors of the development of T2D (13). Of importance, chemerin has been associated with upregulation of IL-1β, TNF-α, IL-6 and MCP-1 (2, 45), an additional and potential mechanism whereby chemerin signals may modulate vascular oxidative stress and altered insulin signaling. TNF-α for example has been identified as a regulator of insulin sensitivity (40). In 3T3-L1 adipocytes, IL-6 reduces expression of insulin receptor substrate (IRS-1) and the glucose transporter GLUT4 (36). Similarly, increased levels of TNF-α reduce IRS-1 phosphorylation and decrease insulin signal transduction in skeletal muscle and adipose tissue from obese rats (18). Accordingly, our data show that chemerin, a pro-inflammatory adipokine, decreases insulin-induced phosphorylation of Akt as well as reduces GLUT4 translocation to the membrane and insulin-induced glucose uptake in VSMC from control mice. Molecular effects of chemerin in vascular insulin signalling

are associated with a decrease in insulin-induced vasodilation, by mechanisms that affect Akt signalling and oxidative status. Together, these findings suggest that the adipokine chemerin confers an insulin resistant phenotype to VSMC.

Corroborating our data, a recent study demonstrated that chemerin decreases glucose uptake and Akt phosphorylation in insulin-stimulated cardiomyocytes (52). Inhibition of ERK1/2 MAPK partially prevented chemerin-induced impairment of Akt phosphorylation and glucose uptake (52). In addition, Jager and colleagues have shown that interleukin-1β (IL-1β) reduces insulin-induced Akt phosphorylation (Thr^{308}). Similarly, IL-1β decreases IRS-1 and Akt protein expression in adipocytes, which leads to lower insulin-induced glucose uptake (19).

Furthermore, db/db mice treated with ChemR23 antagonist (CCX832) present a slight decrease in body weight, supporting the suggestion that chemerin regulates adipogenesis via ChemR23 receptor (34). However, the effects of depletion or inhibition of ChemR23 upon body weight are still controversial. While Rouger *et al* did not observe changes in body weight or fat mass in ChemR23 knockout (KO) mice (37), Ernst and colleagues showed that $CMKLR1^{-/-}$ mice have lower food intake, total body mass, and percent of body fat compared with wild-type controls (9).

In addition to considering ChemR23 blockade effects on body weight, it is important to consider metabolic aspects, such as glucose and insulin levels. CCX832-treated db/db mice exhibited a significant decrease in plasma glucose and insulin levels and HOMA index, strengthening the notion that chemerin contributes to insulin resistance in this model of obesity related to T2D. In addition, cholesterol and triglyceride levels in db/db mice were also reduced by CCX832. Of importance, significantly increased levels of chemerin were observed both in db/db and HFD-treated mice, reinforcing the idea that this adipokine is linked to glucose

390 homeostasis and metabolic disorders in obesity and T2D (10). Ernst and colleagues demonstrated
391 that CMKLR1$^{-/-}$ mice fed with high fat diet present reduced blood glucose and serum insulin.
392 However, CMKLR1 loss is associated with glucose intolerance, which was linked to decreased
393 glucose-stimulated insulin secretion (9). On the other hand, Rouger and colleagues verified that
394 glucose tolerance was not affected in young ChemR23 knockout mice (37).

395 Classically, insulin metabolic signalling results in vasodilatation via increased NO
396 production and production of prostaglandins and endothelium-derived hyperpolarizing factors
397 (30). In addition to reducing insulin-induced vasodilatation in non-obese mice by mechanisms
398 involving PI3K/Akt pathway and oxidative stress, chemerin also reduces eNOS phosphorylation
399 (Ser^{1177}) and decreases insulin-stimulated NO production in endothelial cells, also by oxidative
400 stress-mediated events. These effects of chemerin may be directly involved in vascular insulin
401 dysfunction associated with diabetes and obesity. It has been proposed that resistance to the
402 vascular effects of insulin selectively involves the PI3K/Akt/NO signalling pathway (29). In
403 endothelial cells, blockade of the PI3K pathway induces insulin resistance, which in turn blunts
404 production of NO (28). As demonstrated in this study, most of chemerin effects are mediated by
405 ChemR23 since its antagonism partially restores the decreased insulin-induced vasodilatation in
406 both obesity models, db/db and HFD-fed mice, and also chemerin decreases vascular Akt
407 phosphorylation in db/db mice.

408 Oxidative stress contributes to insulin resistance, particularly in skeletal muscle as well as
409 dysfunction of pancreatic β cells (12). Cellular and systemic disorders that may contribute to
410 overproduction of reactive oxygen species (ROS), including hyperglycaemia, dyslipidaemia,
411 endoplasmic reticulum (ER) stress, advanced glycation end products (AGEs), nitric oxide
412 synthase and lipid peroxides, can activate factors associated with insulin resistance (43). In

humans, there is a positive association between serum markers of oxidative stress and the degree of insulin resistance (32). In experimental animal models, oxidative stress interrupts IRS-1 and PI3K activation induced by insulin, and impairs the translocation of GLUT4 in 3T3-L1 adipocytes (44). In adipose tissue from healthy men with excessive caloric intake, oxidative stress induces insulin resistance partially via carbonylation and oxidation-induced inactivation of GLUT4 (3). Hence, increased ROS generation in vessels from db/db mice may be associated with decreased insulin signalling observed in those animals. In addition, chemerin/ChemR23 axis may contribute to insulin resistance since ChemR23 antagonism attenuates ROS generation and also restores insulin signalling in vessels from db/db mice. Furthermore, our findings clearly show the involvement of oxidative stress upon chemerin-induced insulin signalling impairment since antioxidants attenuate the reduced Akt phosphorylation as well as the decreased glucose uptake and insulin-induced vasodilatation observed in VSMC and arteries challenged with chemerin.

This study also demonstrates that chemerin decreases AMPK phosphorylation both in EC and VSMC. AMPK is a serine-threonine kinase that has emerged as an important mediator of glucose metabolism and AMPK-activating drugs are potentially useful in T2D treatment. It is already established that acute AMPK activation stimulates glucose uptake by skeletal muscle via both GLUT1 and GLUT4 (39). In cardiomyocytes, AMPK activation increases GLUT4 expression in a PKC-dependent manner (31). Moreover, AMPK activation by 5-amino-4-imidazole-1-β-D-carboxamide ribofuranoside (AICAR) increases heart and skeletal muscle glucose uptake (27, 38) possibly by increasing GLUT4 expression (17). Most importantly, overexpression of human GLUT4 gene protects db/db mice from insulin resistance and diabetes (5). Similarly, our findings show that AICAR (and also PI3K/Akt activation) reverses the effects

of chemerin on insulin-induced glucose uptake in VSMC from normal mice, in accordance with the diminished AMPK phosphorylation in response to chemerin.

Crosstalk between GPCRs and tyrosine kinase receptors (RTKs) is increasingly being recognized as a major mechanism regulating complex signalling pathways (25). ChemR23 is an G protein-coupled receptor that acts through G_i to activate various intracellular signalling pathways, such as ERK1/2 (49). The insulin receptor (IR) belongs to the family of RTKs, which play a critical role in development, cell division, and metabolism. Activation of RTK family members results in autophosphorylation and phosphorylation of selective protein substrates (IRS) exclusively on tyrosine residues. Recently, various likely mechanisms for the transactivation between GPCR and RTK have emerged. Molecules such as PKC, Src and ROS as well as adaptor/scaffold proteins such as Gab1, IRS-1, and GIT1 have been implicated as mediators of GPCR-ligand induced RTK transactivation (23). This study shows that chemerin, through ChemR23, modulates IRS-1 serine phosphorylation and the subsequent signalling cascade. Recently, chemerin has been shown to stimulate bone marrow-derived mesenchymal stromal cells migration via ERK1/2, p38MAPK and JNK-II kinases in a PKC-dependent manner (22). A limitation of the present study is that mechanisms underlying ChemR23 and IR/IRS crosstalk have not been explored. Thus, further studies are needed to understand and dissect specific proteins linking ChemR23 and IR/IRS signalling.

In conclusion, our data indicate that the chemerin/ChemR23 system plays an important role in diabetes-associated impaired vascular insulin signalling and oxidative stress, suggesting its involvement in the pathogenesis of vascular insulin resistance. Antagonism of the system ameliorates vascular dysfunction and normalizes insulin signalling in a T2D animal model.

Targeting chemerin/ChemR23 may be an attractive strategy to improve insulin signalling and vascular function in obesity-associated diabetes.

PERSPECTIVES AND SIGNIFICANCE

Adipokines participate in many physiological processes implicated in cardiovascular complications associated with obesity and diabetes. Advances in the understanding of the role of adipocyte-derived factors in obesity-associated vascular dysfunction may uncover mechanisms involved in adiposity-related diseases. Chemerin/ChemR23 system plays an important role in diabetes-associated impaired vascular insulin signalling and oxidative stress, suggesting its involvement in the pathogenesis of vascular insulin resistance. Antagonism of the system ameliorates vascular dysfunction and normalizes insulin signalling in a T2D animal model. We believe that targeting chemerin/ChemR23 may be an attractive therapeutic strategy to improve insulin signalling and vascular function in obesity-associated diabetes.

ACKNOWLEDGEMENTS

We thank ChemoCentryx (Mountain View, CA, USA) for providing the compound CCX832 and consultation; Carla Pavan for the technical support with the animals and Aikaterini Anagnostopoulou for the immunofluorescence support. We also thank Fundação de Amparo à Pesquisa do Estado de São Paulo (FAPESP) [grants 2012/13144-8, 2015/01630-3 and 2013/08216-2, Center of Research in Inflammatory Diseases (CRID)], Coordenação de Aperfeiçoamento de Pessoal de Nível Superior (CAPES) [grant 2053-13-6] and the British Heart Foundation (BHF) [RE/13/5/30177; BHF Chair CH/12/429762] for support this work.

GRANTS

This study was supported by the Fundação de Amparo à Pesquisa do Estado de São Paulo (FAPESP) [grants 2012/13144-8 and 2015/01630-3 to KBN, and 2013/08216-2 to the Center of Research in Inflammatory Diseases – CRID], Coordenação de Aperfeiçoamento de Pessoal de Nível Superior (CAPES) [grant 2053-13-6] and the British Heart Foundation (BHF) [RE/13/5/30177; BHF Chair CH/12/429762].

DISCLOSURES

None.

REFERENCES

1. **Barnea G, Strapps W, Herrada G, Berman Y, Ong J, Kloss B, Axel R, and Lee KJ**. The genetic design of signaling cascades to record receptor activation. *Proceedings of the National Academy of Sciences of the United States of America* 105: 64-69, 2008.

2. **Berg V, Sveinbjornsson B, Bendiksen S, Brox J, Meknas K, and Figenschau Y**. Human articular chondrocytes express ChemR23 and chemerin; ChemR23 promotes inflammatory signalling upon binding the ligand chemerin(21-157). *Arthritis research & therapy* 12: R228, 2010.

3. **Boden G, Homko C, Barrero CA, Stein TP, Chen X, Cheung P, Fecchio C, Koller S, and Merali S**. Excessive caloric intake acutely causes oxidative stress, GLUT4 carbonylation, and insulin resistance in healthy men. *Sci Transl Med* 7: 304re307, 2015.

4. **Bozaoglu K, Bolton K, McMillan J, Zimmet P, Jowett J, Collier G, Walder K, and Segal D**. Chemerin is a novel adipokine associated with obesity and metabolic syndrome. *Endocrinology* 148: 4687-4694, 2007.

5. **Brozinick JT, Jr., McCoid SC, Reynolds TH, Nardone NA, Hargrove DM, Stevenson RW, Cushman SW, and Gibbs EM**. GLUT4 overexpression in db/db mice dose-dependently ameliorates diabetes but is not a lifelong cure. *Diabetes* 50: 593-600, 2001.

6. **da Costa RM, Fais RS, Dechandt CRP, Louzada-Junior P, Alberici LC, Lobato NS, and Tostes RC**. Increased mitochondrial ROS generation mediates the loss of the anti-contractile effects of perivascular adipose tissue in high-fat diet obese mice. *British journal of pharmacology* 174: 3527-3541, 2017.

7. **da Costa RM, Neves KB, Mestriner FL, Louzada-Junior P, Bruder-Nascimento T, and Tostes RC**. TNF-alpha induces vascular insulin resistance via positive modulation of PTEN and decreased Akt/eNOS/NO signaling in high fat diet-fed mice. *Cardiovascular diabetology* 15: 119, 2016.

8. **Dixelius J, Makinen T, Wirzenius M, Karkkainen MJ, Wernstedt C, Alitalo K, and Claesson-Welsh L**. Ligand-induced vascular endothelial growth factor receptor-3 (VEGFR-3) heterodimerization with VEGFR-2 in primary lymphatic endothelial cells regulates tyrosine phosphorylation sites. *The Journal of biological chemistry* 278: 40973-40979, 2003.

9. **Ernst MC, Haidl ID, Zuniga LA, Dranse HJ, Rourke JL, Zabel BA, Butcher EC, and Sinal CJ**. Disruption of the chemokine-like receptor-1 (CMKLR1) gene is associated with reduced adiposity and glucose intolerance. *Endocrinology* 153: 672-682, 2012.

10. **Ernst MC, Issa M, Goralski KB, and Sinal CJ**. Chemerin exacerbates glucose intolerance in mouse models of obesity and diabetes. *Endocrinology* 151: 1998-2007, 2010.

11. **Ernst MC, and Sinal CJ**. Chemerin: at the crossroads of inflammation and obesity. *Trends in endocrinology and metabolism: TEM* 21: 660-667, 2010.

12. **Evans JL, Goldfine ID, Maddux BA, and Grodsky GM**. Oxidative stress and stress-activated signaling pathways: a unifying hypothesis of type 2 diabetes. *Endocrine reviews* 23: 599-622, 2002.

13. **Fain JN, Bahouth SW, and Madan AK**. TNFalpha release by the nonfat cells of human adipose tissue. *Int J Obes Relat Metab Disord* 28: 616-622, 2004.

14. **Goralski KB, McCarthy TC, Hanniman EA, Zabel BA, Butcher EC, Parlee SD, Muruganandan S, and Sinal CJ**. Chemerin, a novel adipokine that regulates adipogenesis and adipocyte metabolism. *The Journal of biological chemistry* 282: 28175-28188, 2007.

15. **Goralski KB, McCarthy TC, Hanniman EA, Zabel BA, Butcher EC, Parlee SD, Muruganandan S, and Sinal CJ**. Chemerin, a novel adipokine that regulates adipogenesis and adipocyte metabolism. *J Biol Chem* 282: 28175-28188, 2007.

16. **Halpern W, Mulvany MJ, and Warshaw DM**. Mechanical properties of smooth muscle cells in the walls of arterial resistance vessels. *The Journal of physiology* 275: 85-101, 1978.

17. **Holmes BF, Kurth-Kraczek EJ, and Winder WW**. Chronic activation of 5'-AMP-activated protein kinase increases GLUT-4, hexokinase, and glycogen in muscle. *J Appl Physiol (1985)* 87: 1990-1995, 1999.

18. **Hotamisligil GS, Peraldi P, Budavari A, Ellis R, White MF, and Spiegelman BM**. IRS-1-mediated inhibition of insulin receptor tyrosine kinase activity in TNF-alpha- and obesity-induced insulin resistance. *Science* 271: 665-668, 1996.

19. **Jager J, Gremeaux T, Cormont M, Le Marchand-Brustel Y, and Tanti JF**. Interleukin-1beta-induced insulin resistance in adipocytes through down-regulation of insulin receptor substrate-1 expression. *Endocrinology* 148: 241-251, 2007.

20. **Karalis KP, Giannogonas P, Kodela E, Koutmani Y, Zoumakis M, and Teli T**. Mechanisms of obesity and related pathology: linking immune responses to metabolic stress. *Febs J* 276: 5747-5754, 2009.

21. **Kougias P, Chai H, Lin PH, Yao Q, Lumsden AB, and Chen C**. Effects of adipocyte-derived cytokines on endothelial functions: implication of vascular disease. *J Surg Res* 126: 121-129, 2005.

22. **Kumar JD, Holmberg C, Kandola S, Steele I, Hegyi P, Tiszlavicz L, Jenkins R, Beynon RJ, Peeney D, Giger OT, Alqahtani A, Wang TC, Charvat TT, Penfold M, Dockray GJ, and Varro A**. Increased expression of chemerin in squamous esophageal cancer myofibroblasts and role in recruitment of mesenchymal stromal cells. *PloS one* 9: e104877, 2014.

23. **Lee J, and Pilch PF**. The insulin receptor: structure, function, and signaling. *Am J Physiol* 266: C319-334, 1994.

24. **Lehrke M, Becker A, Greif M, Stark R, Laubender RP, von Ziegler F, Lebherz C, Tittus J, Reiser M, Becker C, Goke B, Leber AW, Parhofer KG, and Broedl UC**. Chemerin is associated with markers of inflammation and components of the metabolic syndrome but does not predict coronary atherosclerosis. *European journal of endocrinology / European Federation of Endocrine Societies* 161: 339-344, 2009.

25. **Lowes VL, Ip NY, and Wong YH**. Integration of signals from receptor tyrosine kinases and g protein-coupled receptors. *Neuro-Signals* 11: 5-19, 2002.

26. **Matsuzawa Y**. White adipose tissue and cardiovascular disease. *Best practice & research Clinical endocrinology & metabolism* 19: 637-647, 2005.

27. **Merrill GF, Kurth EJ, Hardie DG, and Winder WW**. AICA riboside increases AMP-activated protein kinase, fatty acid oxidation, and glucose uptake in rat muscle. *Am J Physiol* 273: E1107-1112, 1997.

28. **Montagnani M, Golovchenko I, Kim I, Koh GY, Goalstone ML, Mundhekar AN, Johansen M, Kucik DF, Quon MJ, and Draznin B**. Inhibition of phosphatidylinositol 3-kinase enhances mitogenic actions of insulin in endothelial cells. *J Biol Chem* 277: 1794-1799, 2002.

29. **Muniyappa R, and Sowers JR**. Role of insulin resistance in endothelial dysfunction. *Rev Endocr Metab Disord* 14: 5-12, 2013.

30. **Muniyappa R, and Yavuz S**. Metabolic actions of angiotensin II and insulin: a microvascular endothelial balancing act. *Mol Cell Endocrinol* 378: 59-69, 2013.

31. **Nishino Y, Miura T, Miki T, Sakamoto J, Nakamura Y, Ikeda Y, Kobayashi H, and Shimamoto K**. Ischemic preconditioning activates AMPK in a PKC-dependent manner and induces GLUT4 up-regulation in the late phase of cardioprotection. *Cardiovasc Res* 61: 610-619, 2004.

32. **Paolisso G, D'Amore A, Volpe C, Balbi V, Saccomanno F, Galzerano D, Giugliano D, Varricchio M, and D'Onofrio F**. Evidence for a relationship between oxidative stress and insulin action in non-insulin-dependent (type II) diabetic patients. *Metabolism: clinical and experimental* 43: 1426-1429, 1994.

33. **Poirier P, Giles TD, Bray GA, Hong Y, Stern JS, Pi-Sunyer FX, and Eckel RH**. Obesity and cardiovascular disease: pathophysiology, evaluation, and effect of weight loss. *Arteriosclerosis, thrombosis, and vascular biology* 26: 968-976, 2006.

34. **Roh SG, Song SH, Choi KC, Katoh K, Wittamer V, Parmentier M, and Sasaki S**. Chemerin--a new adipokine that modulates adipogenesis via its own receptor. *Biochemical and biophysical research communications* 362: 1013-1018, 2007.

35. **Roh SG, Song SH, Choi KC, Katoh K, Wittamer V, Parmentier M, and Sasaki S**. Chemerin--a new adipokine that modulates adipogenesis via its own receptor. *Biochemical and biophysical research communications* 362: 1013-1018, 2007.

36. **Rotter V, Nagaev I, and Smith U**. Interleukin-6 (IL-6) induces insulin resistance in 3T3-L1 adipocytes and is, like IL-8 and tumor necrosis factor-alpha, overexpressed in human fat cells from insulin-resistant subjects. *The Journal of biological chemistry* 278: 45777-45784, 2003.

37. **Rouger L, Denis GR, Luangsay S, and Parmentier M**. ChemR23 knockout mice display mild obesity but no deficit in adipocyte differentiation. *The Journal of endocrinology* 219: 279-289, 2013.

38. **Russell RR, 3rd, Bergeron R, Shulman GI, and Young LH**. Translocation of myocardial GLUT-4 and increased glucose uptake through activation of AMPK by AICAR. *Am J Physiol* 277: H643-649, 1999.

39. **Rutter GA, Da Silva Xavier G, and Leclerc I**. Roles of 5'-AMP-activated protein kinase (AMPK) in mammalian glucose homoeostasis. *Biochem J* 375: 1-16, 2003.

40. **Sell H, Dietze-Schroeder D, and Eckel J**. The adipocyte-myocyte axis in insulin resistance. *Trends Endocrinol Metab* 17: 416-422, 2006.

41. **Sell H, Laurencikiene J, Taube A, Eckardt K, Cramer A, Horrighs A, Arner P, and Eckel J**. Chemerin is a novel adipocyte-derived factor inducing insulin resistance in primary human skeletal muscle cells. *Diabetes* 58: 2731-2740, 2009.

42. **Shalaby F, Rossant J, Yamaguchi TP, Gertsenstein M, Wu XF, Breitman ML, and Schuh AC**. Failure of blood-island formation and vasculogenesis in Flk-1-deficient mice. *Nature* 376: 62-66, 1995.

43. **Solinas G, and Karin M**. JNK1 and IKKbeta: molecular links between obesity and metabolic dysfunction. *Faseb J* 24: 2596-2611, 2010.

44. **Tirosh A, Potashnik R, Bashan N, and Rudich A**. Oxidative stress disrupts insulin-induced cellular redistribution of insulin receptor substrate-1 and phosphatidylinositol 3-kinase in 3T3-L1 adipocytes. A putative cellular mechanism for impaired protein kinase B activation and GLUT4 translocation. *The Journal of biological chemistry* 274: 10595-10602, 1999.

45. **Waltenberger J, Claesson-Welsh L, Siegbahn A, Shibuya M, and Heldin CH**. Different signal transduction properties of KDR and Flt1, two receptors for vascular endothelial growth factor. *The Journal of biological chemistry* 269: 26988-26995, 1994.

46. **Watts SW, Dorrance AM, Penfold ME, Rourke JL, Sinal CJ, Seitz B, Sullivan TJ, Charvat TT, Thompson JM, Burnett R, and Fink GD**. Chemerin connects fat to arterial contraction. *Arteriosclerosis, thrombosis, and vascular biology* 33: 1320-1328, 2013.

47. **Weigert J, Neumeier M, Wanninger J, Filarsky M, Bauer S, Wiest R, Farkas S, Scherer MN, Schaffler A, Aslanidis C, Scholmerich J, and Buechler C**. Systemic chemerin is related to inflammation rather than obesity in type 2 diabetes. *Clin Endocrinol (Oxf)* 72: 342-348, 2010.

48. **Wilcox G**. Insulin and insulin resistance. *Clin Biochem Rev* 26: 19-39, 2005.

49. **Wittamer V, Franssen JD, Vulcano M, Mirjolet JF, Le Poul E, Migeotte I, Brezillon S, Tyldesley R, Blanpain C, Detheux M, Mantovani A, Sozzani S, Vassart G, Parmentier M, and Communi D**. Specific recruitment of antigen-presenting cells by chemerin, a novel

processed ligand from human inflammatory fluids. *The Journal of experimental medicine* 198: 977-985, 2003.

50. **Wittamer V, Gregoire F, Robberecht P, Vassart G, Communi D, and Parmentier M**. The C-terminal nonapeptide of mature chemerin activates the chemerin receptor with low nanomolar potency. *The Journal of biological chemistry* 279: 9956-9962, 2004.

51. **Yamawaki H**. Vascular effects of novel adipocytokines: focus on vascular contractility and inflammatory responses. *Biological & pharmaceutical bulletin* 34: 307-310, 2011.

52. **Zhang R, Liu S, Guo B, Chang L, and Li Y**. Chemerin induces insulin resistance in rat cardiomyocytes in part through the ERK1/2 signaling pathway. *Pharmacology* 94: 259-264, 2014.

FIGURES LEGENDS

Figure 1. Chemerin decreases insulin-induced vasodilatation via ChemR23, Akt/NO and oxidative stress-dependent mechanisms. Endothelium-intact mesenteric arteries from C57BL/6J mice were incubated with chemerin (0.5 ng/mL) or vehicle for one hour. Relaxation response to insulin was evaluated in the absence (A) and in the presence of (B) CCX832 (ChemR23 antagonist), (C) YS-49 (PI3K activator) or (D) Tiron (ROS scavenger), which were added 30 min before the vehicle or chemerin. Vehicle and chemerin curves in A-D were originated from the same sets of experiments. (E) Phosphorylation of eNOS (Ser^{1177}) was determined by western blot in endothelial cells stimulated with chemerin (0.5 ng/mL, one hour) and insulin (30 min) in the absence or presence of CCX832, NAC (ROS scavenger) or 740Y-P (PI3K activator). Values were normalized by total NOS expression. (F) Nitric oxide (NO)

production was determined by DAF2-DA fluorescence in endothelial cells and values were normalized by protein amount. Results represent the mean ± SEM of 5 to 6 experiments. Data were analyzed using one-way ANOVA followed by a post hoc Tukey test. * $p<0.05$ *vs*. vehicle; # $p<0.05$ *vs.* chemerin; σ *vs*. insulin, φ *vs*. chemerin + insulin.

Figure 2. Chemerin decreases vascular insulin signalling in VSMC. Phosphorylation of Akt (A), GLUT4 translocation to the membrane (B), phosphorylation of AMPK in VSMC (C) and HMEC (D) were determined by western blot. Cells were pre-treated with CCX832, NAC or 740Y-P, added 30 min before the stimulation with chemerin and/or insulin. Values were normalized by total protein or Na^+/K^+ ATPase. To keep the same sequence of experimental groups in all graphs, representative western blot figures for Akt were spliced as indicated (C). Data represent the mean ± SEM of 4 to 6 experiments. Data were analyzed using one-way ANOVA followed by a post hoc Tukey test or *t*-test. * $p<0.05$ vs. vehicle; # $p<0.05$ vs. chemerin, σ $p<0.05$ vs. insulin, φ $p<0.05$ vs. chemerin + insulin.

Figure 3. Chemerin reduces insulin-stimulated glucose uptake in VSMC. 2-Deoxyglucose (2-DG) uptake was measured by exposing VSMC to 2 μCi/ml 2-[^{3}H] DG in the presence of unlabelled 2-DG. Cells were treated with chemerin, Tiron, AICAR (AMPK activator), CCX832 and 740Y-P prior to the stimulation with insulin. Values represent the mean ± SEM of 5 to 6 experiments. Data were analyzed using one-way ANOVA followed by a post hoc Tukey test. * $p<0.05$ *vs*. vehicle, # $p<0.05$ *vs*. chemerin.

Figure 4. ChemR23 antagonism decreases body weight and insulin and glucose levels in db/db mice. (A) Plasma levels of chemerin were measured by ELISA in db/m and db/db mice. (B) Body weight of untreated, vehicle-treated and CCX832-treated db/m and db/db mice was measured along three weeks of treatment. Glucose (C) and insulin (D) levels in vehicle- and CCX832-treated db/m and db/db mice. (E) Insulin sensitivity, calculated using the HOMA-IR index, cholesterol (F) and triglyceride (G) levels in vehicle- and CCX832-treated db/m and db/db mice. Values represent the mean ± SEM of 5 to 8 experiments. Data were analyzed using one-way ANOVA followed by a post hoc Tukey test or *t*-test. * $p<0.05$ *vs*. db/m, ∞ $p<0.05$ *vs*. db/db vehicle.

Figure 5. CCX832 attenuates vascular insulin dysfunction in db/db and HFD-fed mice. Concentration-effect curves to insulin (A) were performed in mesenteric arteries from vehicle- and CCX832-treated db/m and db/db mice. Phosphorylation of Akt (B) in aorta from vehicle and CCX832-treated db/m and db/db mice was determined by western blot. Values were normalized by total protein expression. (C) Plasma levels of chemerin were measured by ELISA in control diet or HFD- fed mice. (D) Concentration-effect curves to insulin were performed in mesenteric arteries from control diet- and HFD-treated mice. Curves were performed in the presence and absence of CC832 added 30 minutes prior curves. Results represent the mean ± SEM of 5 to 8 experiments. Data were analyzed using one-way ANOVA followed by a post hoc Tukey test or *t*-test. * $p<0.05$ *vs*. db/m, ∞ $p<0.05$ *vs*. db/db vehicle; ϴ $p<0.05$ *vs*. control diet, † $p<0.05$ *vs*. HFD.

Figure 6. CCX832 reduces vascular oxidative stress in db/db mice. (A) Representative images and (B) quantitative analysis of 8-OHG-positive nuclei in endothelium-intact aorta from vehicle and CCX832-treated db/m and db/db mice. Scale bar = 20 μm; 40X. Results represent

the mean ± SEM of 5 experiments. Data were analyzed using one-way ANOVA followed by a post hoc Tukey test or *t*-test. * $p<0.05$ *vs*. db/m, ∞ $p<0.05$ *vs*. db/db vehicle.

Figure 1.

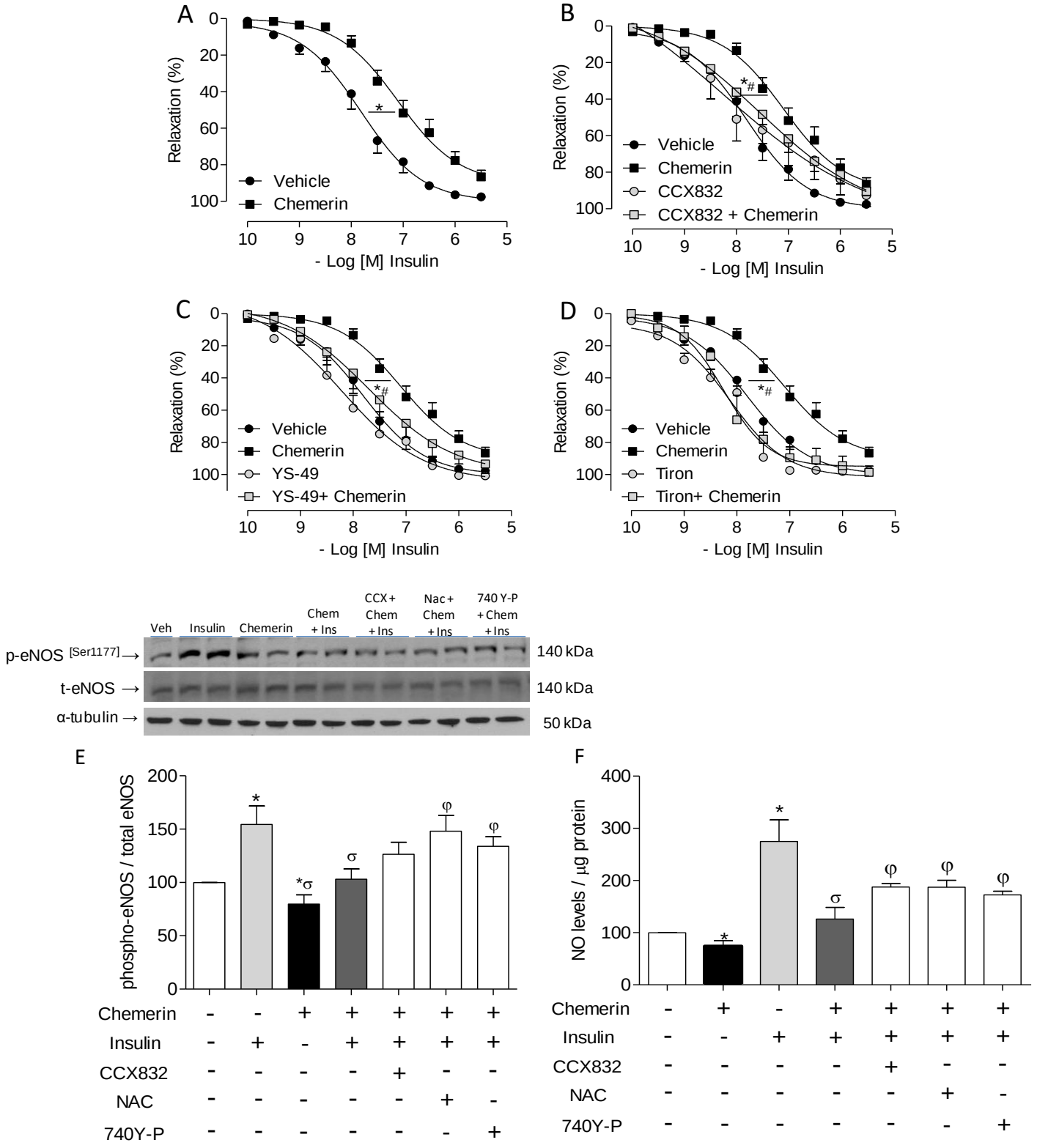
A
Relaxation (%)
- Log [M] Insulin
Vehicle
Chemerin
B
CCX832
CCX832 + Chemerin
C
YS-49
YS-49+ Chemerin
D
Tiron
Tiron+ Chemerin
Veh
Insulin
Chemerin
Chem + Ins
CCX + Chem + Ins
Nac + Chem + Ins
740 Y-P + Chem + Ins
p-eNOS [Ser1177]
t-eNOS
α-tubulin
140 kDa
140 kDa
50 kDa
E
phospho-eNOS / total eNOS
Chemerin
Insulin
CCX832
NAC
740Y-P
F
NO levels / µg protein

Figure 2.

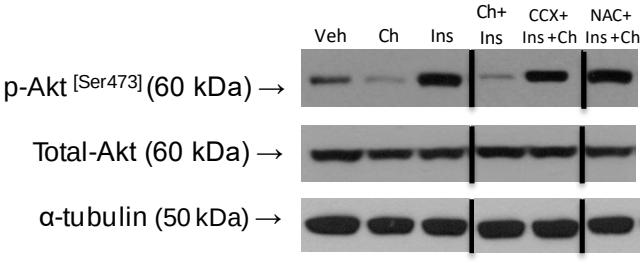
Veh
Ch
Ins
Ch+ Ins
CCX+ Ins +Ch
NAC+ Ins +Ch
p-Akt [Ser473] (60 kDa) →
Total-Akt (60 kDa) →
α-tubulin (50 kDa) →

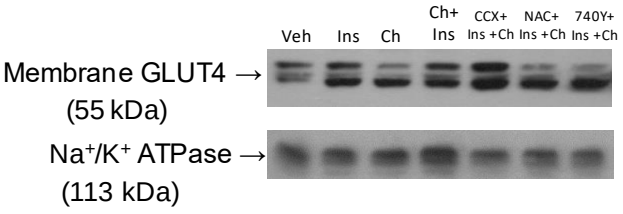
Veh
Ins
Ch
Ch+ Ins
CCX+ Ins +Ch
NAC+ Ins +Ch
740Y+ Ins +Ch
Membrane GLUT4 → (55 kDa)
Na+/K+ ATPase → (113 kDa)

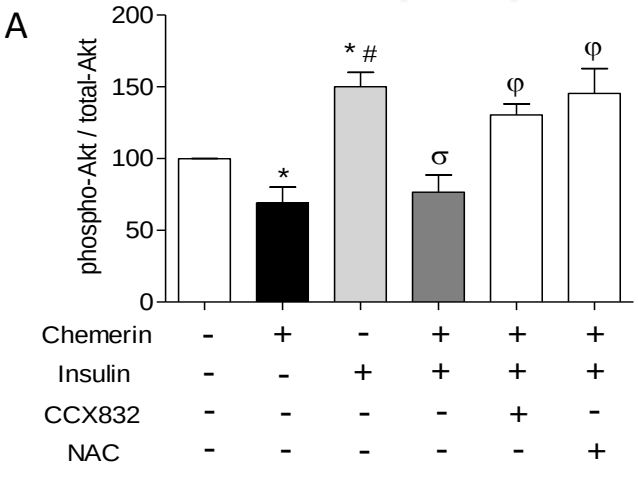
A
phospho-Akt / total-Akt
200
150
100
50
0
Chemerin - + - + + +
Insulin - - + + + +
CCX832 - - - - + -
NAC - - - - - +

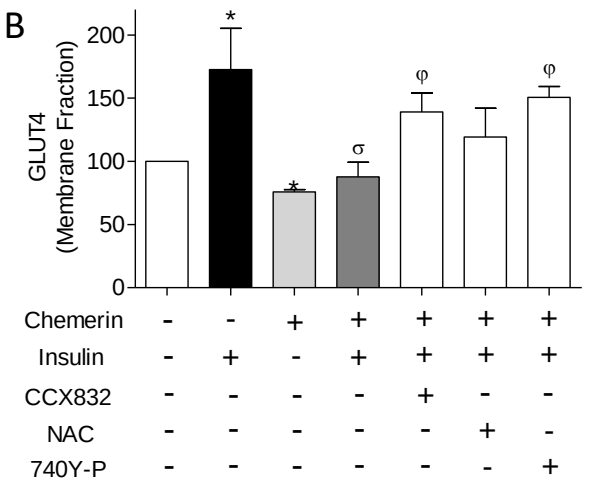
B
GLUT4 (Membrane Fraction)
200
150
100
50
0
Chemerin - - + + + + +
Insulin - + - + + + +
CCX832 - - - - + - -
NAC - - - - - + -
740Y-P - - - - - - +

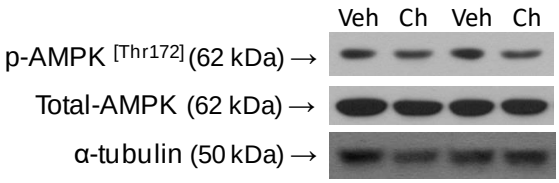
Veh
Ch
Veh
Ch
p-AMPK [Thr172] (62 kDa) →
Total-AMPK (62 kDa) →
α-tubulin (50 kDa) →

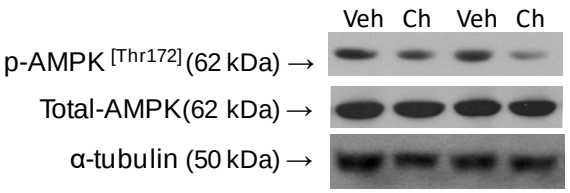
Veh
Ch
Veh
Ch
p-AMPK [Thr172] (62 kDa) →
Total-AMPK(62 kDa) →
α-tubulin (50 kDa) →

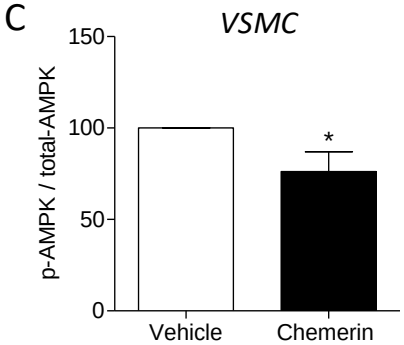
C
VSMC
p-AMPK / total-AMPK
150
100
50
0
Vehicle
Chemerin

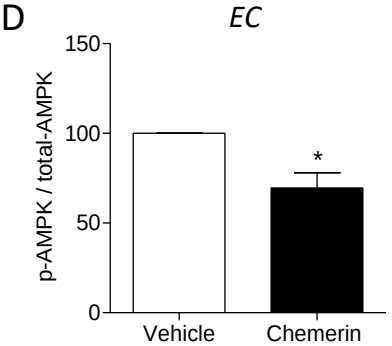
D
EC
p-AMPK / total-AMPK
150
100
50
0
Vehicle
Chemerin

Figure 3.

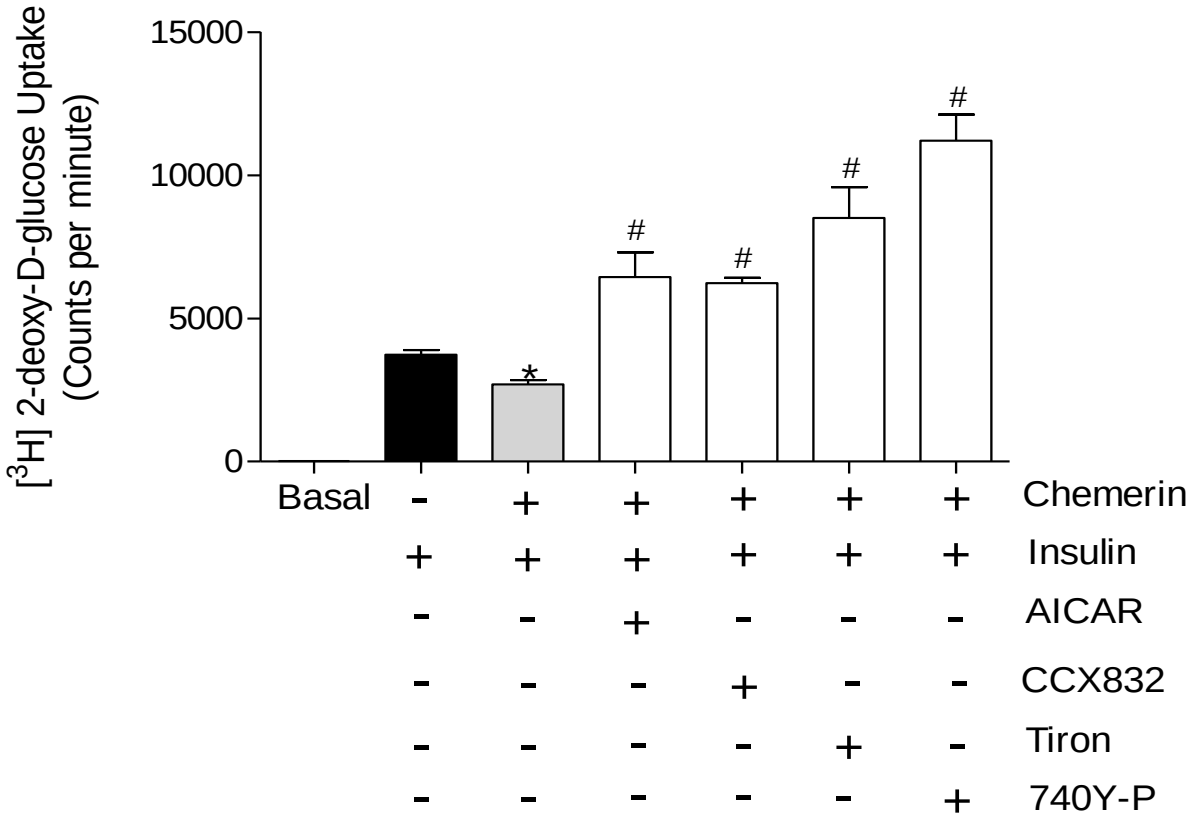
[3H] 2-deoxy-D-glucose Uptake
(Counts per minute)
15000
10000
5000
0
*
#
#
#
#
Basal
Chemerin
Insulin
AICAR
CCX832
Tiron
740Y-P

Figure 4.

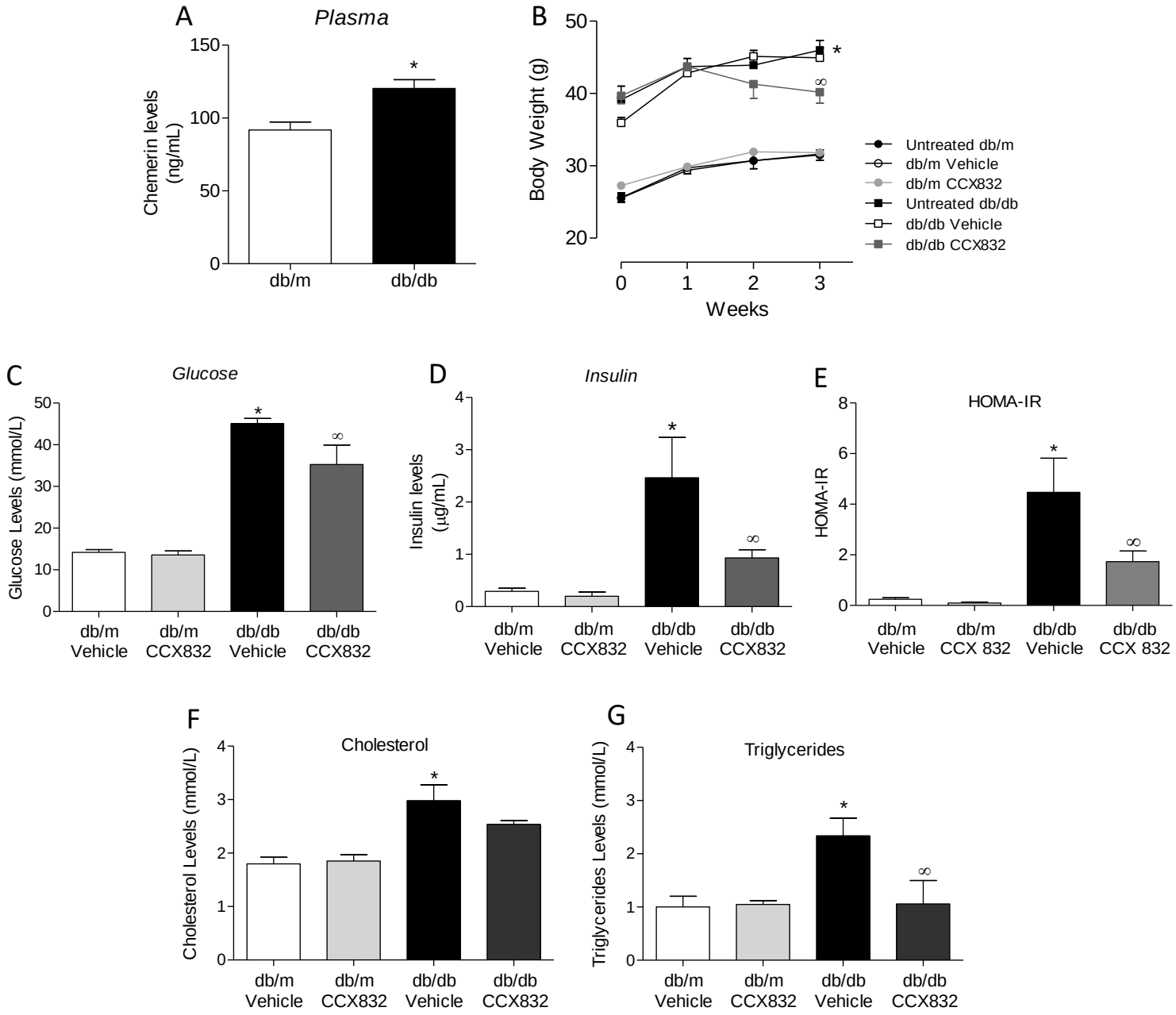
A
Plasma
Chemerin levels (ng/mL)
150
100
50
0
*
db/m
db/db
B
Body Weight (g)
50
40
30
20
0
1
2
3
Weeks
*
∞
Untreated db/m
db/m Vehicle
db/m CCX832
Untreated db/db
db/db Vehicle
db/db CCX832
C
Glucose
Glucose Levels (mmol/L)
50
40
30
20
10
0
*
∞
db/m Vehicle
db/m CCX832
db/db Vehicle
db/db CCX832
D
Insulin
Insulin levels (µg/mL)
4
3
2
1
0
*
∞
db/m Vehicle
db/m CCX832
db/db Vehicle
db/db CCX832
E
HOMA-IR
HOMA-IR
8
6
4
2
0
*
∞
db/m Vehicle
db/m CCX 832
db/db Vehicle
db/db CCX 832
F
Cholesterol
Cholesterol Levels (mmol/L)
4
3
2
1
0
*
db/m Vehicle
db/m CCX832
db/db Vehicle
db/db CCX832
G
Triglycerides
Triglycerides Levels (mmol/L)
4
3
2
1
0
*
∞
db/m Vehicle
db/m CCX832
db/db Vehicle
db/db CCX832

Figure 5.

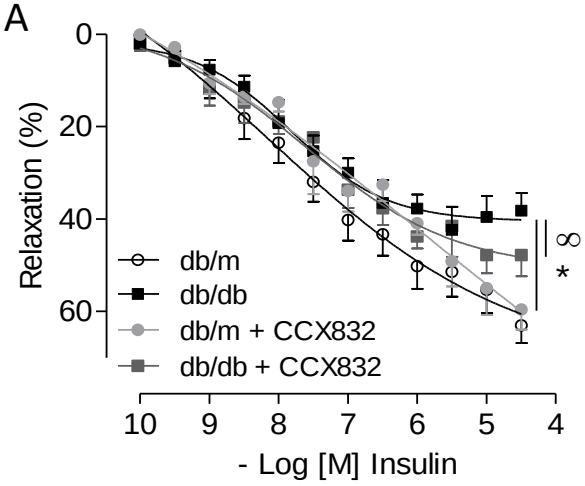
A
Relaxation (%)
0
20
40
60
db/m
db/db
db/m + CCX832
db/db + CCX832
10 9 8 7 6 5 4
- Log [M] Insulin
∞
*

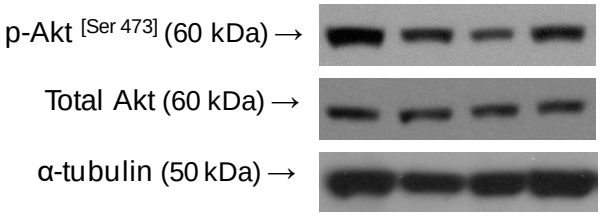
p-Akt [Ser 473] (60 kDa) →
Total Akt (60 kDa) →
α-tubulin (50 kDa) →

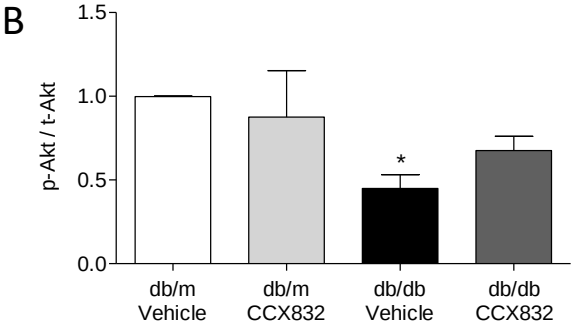
B
p-Akt / t-Akt
1.5
1.0
0.5
0.0
*
db/m Vehicle
db/m CCX832
db/db Vehicle
db/db CCX832

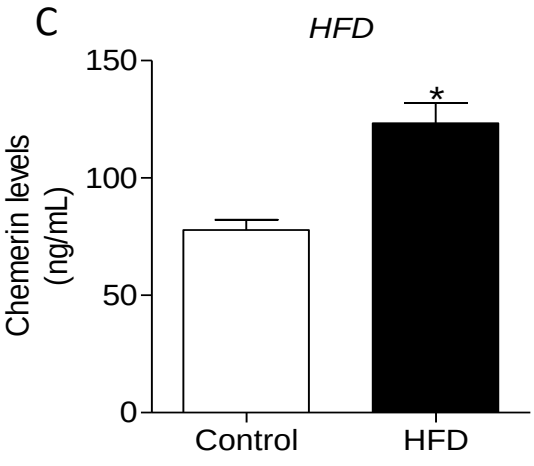
C
HFD
Chemerin levels (ng/mL)
150
100
50
0
*
Control
HFD

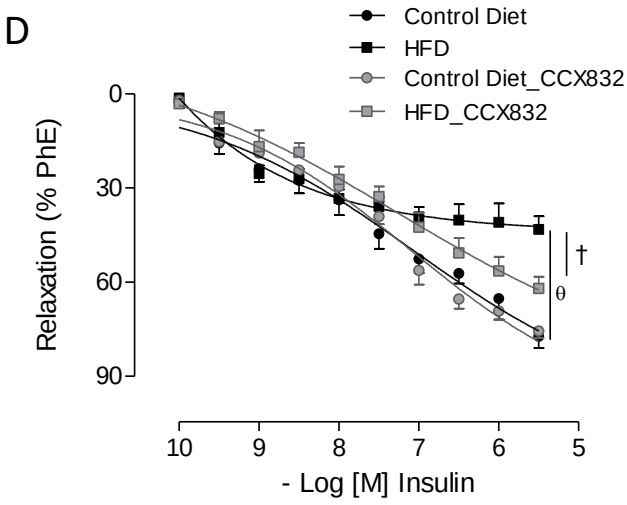
D
Control Diet
HFD
Control Diet_CCX832
HFD_CCX832
Relaxation (% PhE)
0
30
60
90
10 9 8 7 6 5
- Log [M] Insulin
†
θ

Figure 6.

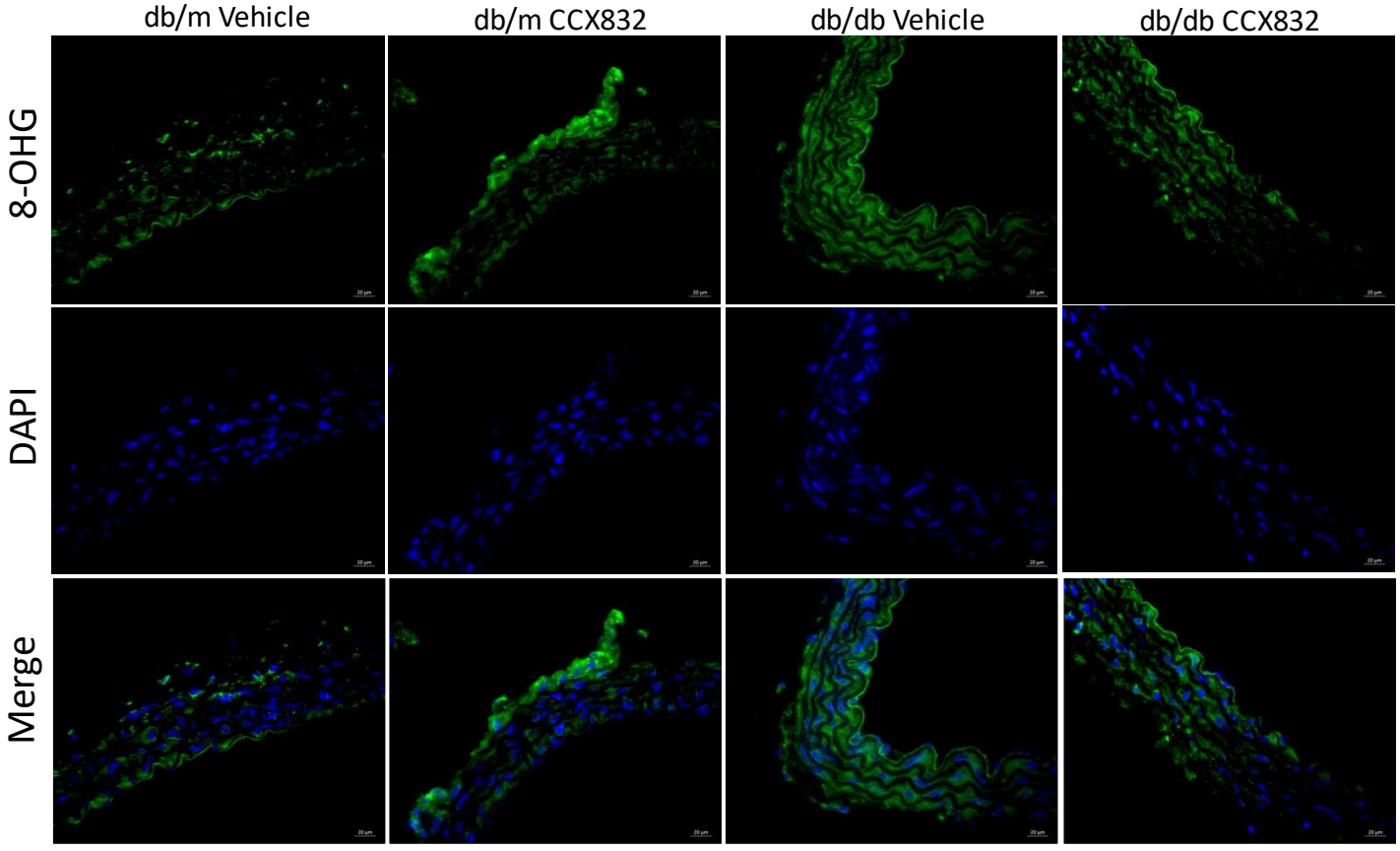
db/m Vehicle
db/m CCX832
db/db Vehicle
db/db CCX832
8-OHG
DAPI
Merge

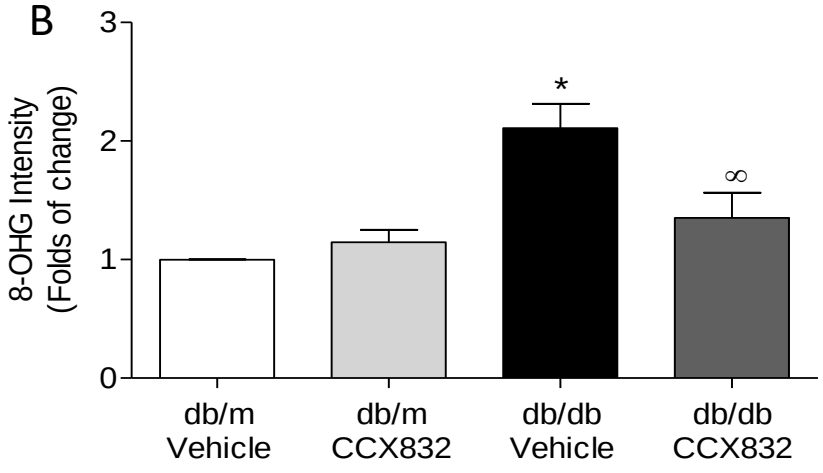
B
8-OHG Intensity
(Folds of change)
3
2
1
0
*
∞
db/m
Vehicle
db/m
CCX832
db/db
Vehicle
db/db
CCX832